Fuel 357 (2024) 129975

Contents lists available at ScienceDirect

Fuel

journal homepage: www.elsevier.com/locate/fuel

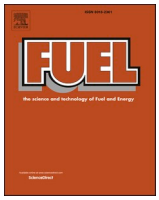

Full Length Article

Numerical modeling of plasma assisted ignition of $CH_4/O_2/He$ mixture by the nanosecond repetitive pulsed surface dielectric barrier discharge

Ziying Xin [a], Zhencao Zheng [a], Yong Hu [a], Ao Sun [a], Feiyang Zhao [a,b,*], Wenbin Yu [a,b,*]

[a] School of Energy and Power Engineering, Shandong University, Jinan, Shandong 250061, China
[b] Shenzhen Research Institute of Shandong University, Shenzhen, Guangdong 518057, China

ARTICLE INFO

Keywords:
Non-equilibrium plasma
Plasma assisted ignition
Plasma kinetic mechanism
Path analysis
Methane combustion

ABSTRACT

A nanosecond repetitive pulsed surface dielectric barrier discharge (NRP-SDBD) is a promising method for generation of non-equilibrium plasma with more kinetic activity. This paper presents numerical studies on the effects of pulse repetition frequency (PRF) on low temperature ignition of lean and stoichiometric $CH_4/O_2/He$ mixture in NRP-SDBD plasma. A skeletal plasma kinetics mechanism is primary developed and calibrated, to mitigate the computational loads of modeling SDBD discharge by the two-dimensional plasma solver PASSKEy coupled with Poisson's equation. The discharge current was well predicted, meanwhile the sequential and spatial reduced electric field (E/N) is revealed as the ionization wave propagates forward. Special attention is placed on time-evolution of electric field strength used as inputs in simulation of plasma assisted ignition (PAI) conducted by zero-dimensional ZDPlasKin-CHEMKIN code. The principle of PAI on lean and stoichiometric $CH_4/O_2/He$ mixture via varied PRF is analyzed in details from view of plasma kinetics and chemical kinetics. Ultimately, the important role of plasma active species O, O(1D), $O_2(a^1\Delta_g)$ on promoting ignition chain reactions is highlighted. It is also concluded that high PRF is beneficial for the accumulation of short lifetime species such as CH_4(v13) and O(1D), which participate in the formation of important intermediate CH_3.

1. Introduction

With the continuous depletion of fossil fuels and the increasingly strict emission regulations, seeking suitable alternative fuels and developing new technologies for clean and efficient combustion have attracted more attention. Natural gas is considered to be one of the most promising alternative fuels for Internal combustion engines (ICEs) owing to its abundant reserves, low-carbon content and better anti-knock performance due to its higher octane number, hence higher compression ratios is acceptable in natural gas fueled-engine. However, natural gas and syngas have high auto-ignition temperature, hence it would only be ignited by combustion of pilot fuel such as diesel with high reactivity or high energetic ignition systems, to break stable C—H bond of methane [1]. In addition, natural gas lean combustion in spark-ignited engines has remarkable advantages of improved thermal efficiency while keeping ultra-low emission levels. Nevertheless, negative cycle-to-cycle variability or even misfires are the main challenges caused by excessive lean mixture combustion. To overcome the combustion instability, the more robust and energetic ignition technology is the key issue to constantly improve the thermal efficiency of natural gas fuel engines.

Plasma is generated when the electrons are run away from the atoms forming an ionized gas, in which there are roughly equal numbers of positively and negatively charged particles. Plasma assisted combustion/ignition (PAC/PAI) is a promising technology due to specified effect. The first is thermal effect: plasma can quickly increase the temperature of the mixture by transferring electron energy into the surrounding gas, thus improving chemical reaction rates according to the Arrhenius equation. The second is kinetic effect, in which plasma generate active radicals and excited species by collision between high-energy electrons and air/fuel molecules, while the participation of active particles as ignition promoters rapidly accelerates chemical reactions. The third enhancement pathway is transport effect, which refers to the ion wind generated by the plasma accelerates the mixing of reactants [2–4].

Plasma can be classified into equilibrium and non-equilibrium plasma based on its thermodynamic properties. Thermal or equilibrium plasma is characterized by high energy density and equality in between the temperature of electrons and heavy particles. While conversely a non-equilibrium plasma is considered as a lower pressure

* Corresponding authors at: School of Energy and Power Engineering, Shandong University, Jinan, Shandong 250061, China.
E-mail addresses: fyzhao@sdu.edu.cn (F. Zhao), wbyu@sdu.edu.cn (W. Yu).

https://doi.org/10.1016/j.fuel.2023.129975
Received 20 July 2023; Received in revised form 21 September 2023; Accepted 26 September 2023
Available online 6 October 2023
0016-2361/© 2023 Elsevier Ltd. All rights reserved.

Table 1
Species for consumption path flux analysis and the number of reactions retained in the skeletal mechanism.

Type of species	Plasma species	The number of reactions retained in the skeletal mechanism
Vibrationally excited species	O_2(v1), CH_4(v13), CH_4(v24)	from 332 to 190
Dissociative species	O(1D)	from 190 to 176
Positive ions	O_2^+, O^+, CH_4^+, CH_3^+, CH_2^+, He^+	from 176 to 158
Electronically excited species	O_2(A1), O_2(B1), O_2^*, He*	from 158 to 116
Negative ion	O^-, O_2^-, OH^-	from 116 to 91

plasma with low ion and neutral temperatures. The inelastic collision between high-energy electrons and reactant can effectively increase the internal energy of gas or excite gas molecules to higher energy levels, and a large number of strong oxidizing free radicals would be rapidly generated in the reaction system by relaxation or breaking of molecular bonds, which play the role of "chemical combustion promoters". Non-equilibrium plasma has great potential in promoting ignition, enhancing combustion [5,6], extending flammability limits [7], improving flame stability [8], accelerating low-temperature fuel oxidation [9], and fuel reforming [10,11].

Non-equilibrium plasma can be produced by corona discharge [12,13], microwave assisted discharge [14], dielectric barrier discharge (DBD) [15,16], nanosecond pulse discharge [17], etc. Among them, the surface dielectric barrier discharge (SDBD) [18–20]excited by a short pulse with duration of tens of nanoseconds facilitates producing a large area of non-equilibrium plasma, but a relatively high voltage-amplitude pulse is required. Many experiments had been carried out to study the effects of pulse repetition frequency (PRF) on the nanosecond SDBD. Nanosecond repetitively pulsed (NRP) discharge had been proven to support low-amplitude and high-frequency nSDBD with a larger range of non-equilibrium plasma superior to high-amplitude and single-pulse nSDBD [21]. The experiments conducted in dry air at the atmospheric pressure by Abdelaziz A A et al. [22] showed that the currents of NRP-SDBDs are much denser and have higher amplitudes at high PRF.

In order to further explore the underlying physical–chemical mechanism of non-equilibrium PAC/PAI, computer-based tools and numerical simulations are basically needed. Zembi J et al. [23] compared combustion effects of Standard European Gasoline generated by spark and corona ignition using CONVERGE CFD software. It was showed that the important role of O atoms on improving burning rate was stimulated by a corona discharge in the initial stage of the combustion. Mao et al. [24,25] studied ignition enhancement effects of non-equilibrium plasma on CH_4/O_2/He and H_2/O_2/He mixture using hybrid repetitive nanosecond and Direct Current (DC) discharge via hybrid ZDPlasKin-CHEMKIN code. The reduced electric field (E/N, where E is the electric field and N is the gas number density) was set as a square wave based on experimental conditions and used as model input. It was found $O_2(a^1\Delta_g)$ was produced more efficiently in mixed excitation than pure nanosecond pulse discharge, which ultimately favoring shortened ignition delay time. The effect of NRP discharges on the ignition characteristics of NH_3/O_2/He mixtures from medium to high temperature (600–1500 K) at atmospheric pressure was investigated by Galia Faingold et al. [26] using the ZDPlasKin-CHEMKIN coupled model. It was concluded that high-frequency pulses promoted the generation of OH, thus accelerating chain-initiation and branching reactions. The concept of thermal-chemical instability of weakly ionized plasma was put forward by Zhong et al. [27], and one-dimensional numerical model was established to perform transition from the homogeneous to filamentary states coupled with plasma dynamics and chemical kinetics reactions. The results showed that plasma destabilization may occur due to the positive feedback between the change in electron density, E/N, etc. The combustion kinetics reactions can either decelerate or accelerate the occurrence of instability. Under atmospheric pressure, plasma breakdown mainly occurs in the streamer and relies on the enhanced local electric field. The E/N will change rapidly with the propagation of the streamer throughout actual nSDBD. The E/N is a significant parameter during plasma discharge, since it determines the mean electron energy

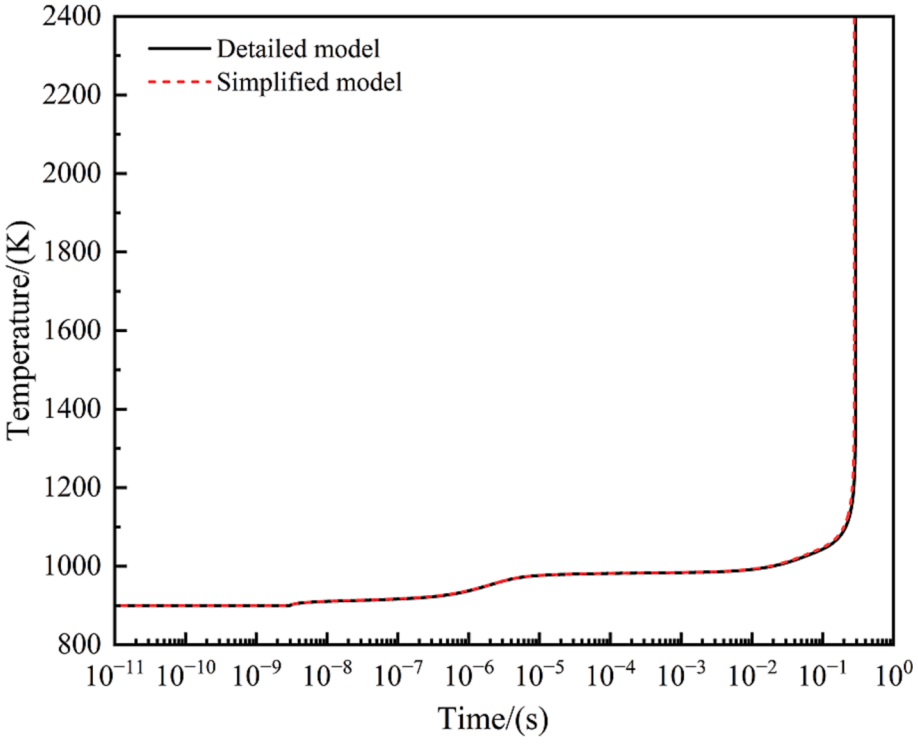

Fig. 1. Time evolution of gas temperature calculated by the simplified and detailed plasma kinetic models in a stoichiometric CH_4/O_2 mixture with 75% helium dilution at 900 K and atmospheric pressure.

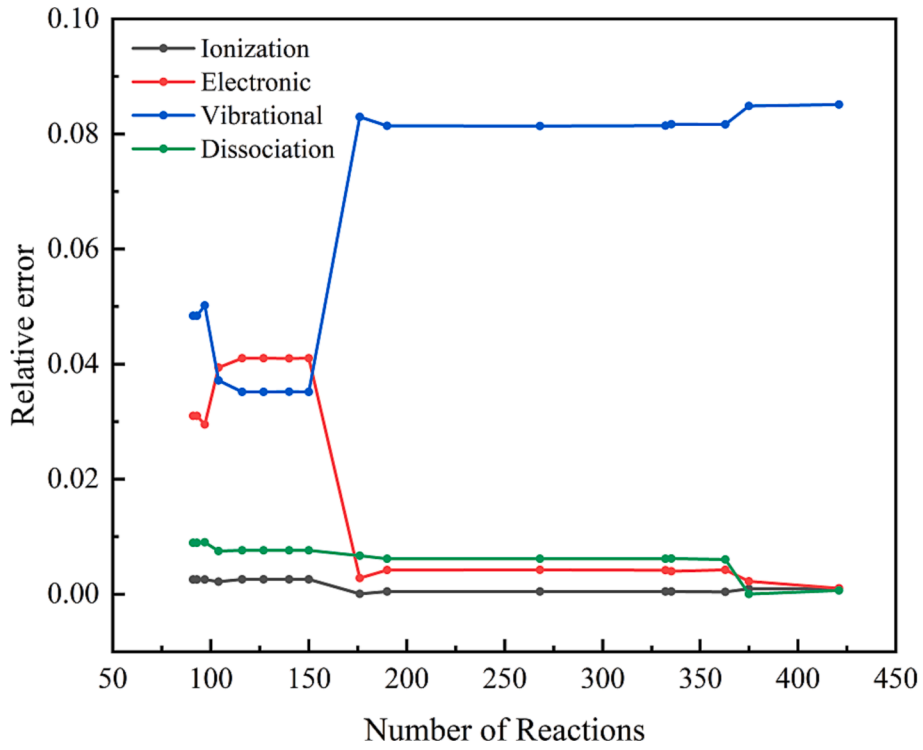

Fig. 2. The relative error in Ω_i as a function of the number of reactions retained in the skeletal mechanism.

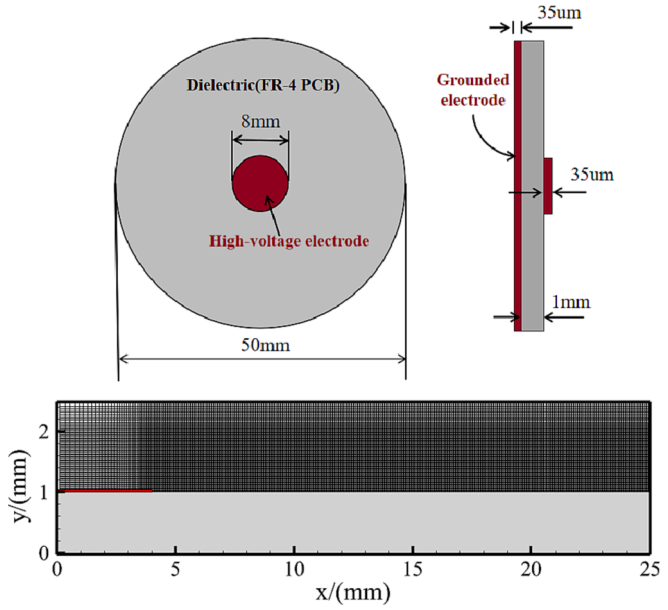

Fig. 3. The schematic diagram of electrode shape, computational domain and mesh distribution.

and controls energy transfer as well as the way or the type of excited state species produced. As a result, multi-dimensional modeling coupled with Poisson's equation for accurate description of the electric field strength is indispensable in plasma simulations. A two-dimensional parallel streamer solver called PASSKEy (Parallel Streamer Solver with KinEtics) was proposed to perform the spatial–temporal evolution of the electric field, species densities, etc during plasma discharge process, and the solver had been elaborately verified in streamer morphology, electron density and current [28–31]. Chen et al. [32] and Mao et al. [33] applied PASSKEy code on studying plasma kinetics mechanisms responsible for steamer-to-spark transition under different gas media and electrode shapes. Recent, a multi-scale adaptive reduced chemistry solver integrated PASSKEy and unsteady reactive flow solver ASURF + was proposed by Mao X et al. [34]. The solver was employed to investigate the effects of NRP frequency, pulse number and flow velocity on the critical ignition volume and minimum ignition energy of H_2/air mixture at 300 K and atmospheric pressure. It provides a new insight for the optimization of PAI in a reactive flow.

Based on the above discussion, the aim of this study is to explore the underlying kinetic mechanism of non-equilibrium PAI on lean methane mixture via SDBD discharge driven by NRP. Firstly, a skeletal plasma kinetic mechanism of CH_4/O_2/He is developed and validated by energy branching of the plasma discharge and flame temperature. Secondly, coupled with plasma kinetic, modeling on the propagation of the streamer initiated by nSDBD is carried on through two-dimensional discharge model, in which the current and sequential E/N are predicted. Subsequent numerical studies on PAI of lean and stoichiometric CH_4/O_2/He mixtures are conducted via zero-dimensional ZDPlasKin-CHEMKIN model. The effects of plasma discharge configurations on stimulating ignition of varied CH_4/O_2/He mixtures are systematically analyzed in the aspects of plasma physics kinetic and chemical reaction kinetic.

2. Simplify plasma dynamics mechanism based on P-DRGEP method

The detailed kinetics mechanism of non-equilibrium plasma assisted CH_4/O_2/He mixture combustion consists of a plasma kinetic sub-model with 629 reactions developed by Mao et al. [25] and a chemistry kinetic sub-model with 649 reactions developed by J.K. Lefkowitz et al. [35]. Such a large-sized detailed mechanism is inapplicable to simulate unsteady multi-dimensional plasma discharges due to its high computational cost. Aurélie Bellemans et al. [36] proposed a novel reduction method Plasma-targeted Directed Relation Graph with Error Propagation (P-DRGEP) in which energy branching characteristic of plasma discharges was introduced. The energy branching describes electronic

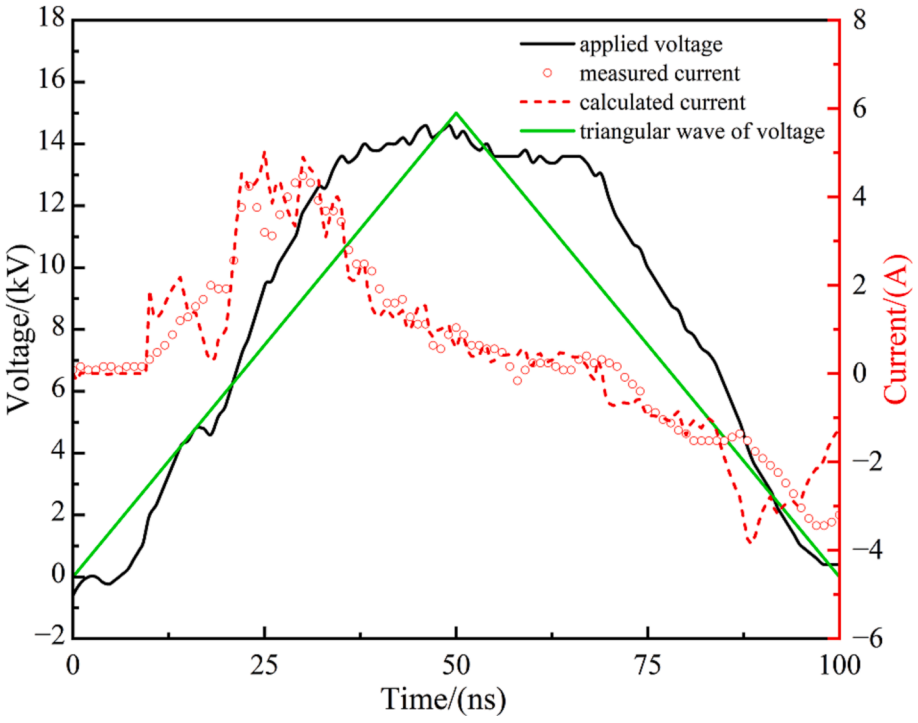

Fig. 4. The applied voltage, the experimentally measured and calculated current by PASSKEy.

energy loss in different classes of electron impact reactions. In this section, a skeletal plasma kinetic model of CH_4/O_2/He mixture is proposed from the detailed plasma sub-model based on P-DRGEP method. The combustion sub-mech remains the same as the detailed one during the simplification process.

DRGEP defines the direct interaction coefficient r_{AB} which quantifies coupling relationship between a target species A and B. The most commonly used targets include fuels, oxidants, important combustion intermediates and products. r_{AB} is defined as

$$r_{AB} = \frac{\left|\sum_{r\in R} v_{r,A} q_r \delta_B^r\right|}{\max(P_A, C_A)} \tag{1}$$

where R is the elementary reaction series in detailed mechanism, $v_{r,A}$ is the net stoichiometric coefficient of a species A in the reaction r, q_r is the net chemical reaction rate of the reaction r, δ_B^r is equal to 1 if A and B participate in the reaction r simultaneously, and otherwise it equals to 0. P_A and C_A are the total production and consumption rates of species A, respectively.

P-DRGEP uses energy transfer variables Ω_i as plasma-specific targets, Ω_i is given by Eq.(2). The direct interaction coefficient between any species B and the energy transfer variable Ω_i is expressed as $r_{i,B}$. where i={ion, ele, vib, dis}, E_r is the ionization or excitation energy, N_A is the Avogadro number, q_r is the net rate of reaction r.

$$\Omega_i = \sum_{r\in R_i} - N_A q_r E_r \tag{2}$$

$$r_{i,B} = \frac{\left|\sum_{r\in R_i} \Omega_r \delta_B^r\right|}{|\Omega_i|} \tag{3}$$

2.1. Simplified process and validation of simplified plasma kinetic model

In the current study, the PAI simulation is conducted in a stoichiometric CH_4/O_2 mixture with 75% helium dilution at 900 K and atmospheric pressure via zero-dimensional ZDPlasKin-CHEMKIN coupled model. A hybrid nanosecond discharge with a reduced electric field of 180 Td and a pulse width of 3 ns is applied, thereafter there is a DC discharge with a reduced electric field of 10 Td. CH_4, O_2, O, H, OH, CO, CO_2, e and the energy transfer variables Ω_i are selected as targets and P-DRGEP method is performed via MATLAB code to calculate the direct interaction coefficient between plasma species and the simplified targets. Appropriate thresholds are set to evaluate whether a species should be removed or retained. As a result, eleven species including O_2(v2), O_2(v3), O_2(v4), O_3, O(1S), HCO^+, H_3O^+, $C_2H_3O^+$, CH_5O^+, O_3^-, CO_3^- and 297 plasma related reactions are eliminated from the detailed mechanism. Then further simplification is carried on by consumption path flux analysis for species which have significant impact on energy branching characteristics as shown in Table 1. Finally, a skeletal plasma kinetic mechanism of CH_4/O_2/He containing 91 reactions is well established for modeling plasma discharge, which incorporates electron impact vibrational excitation, electronic excitation, dissociation, ionization and attachment, as well as quenching of excited species et al (Details are given in supplementary materials). The predicted profile of temperature during PAI on stoichiometric CH_4/O_2 mixture is plotted in Fig. 1. Additionally, the mole fractions of target species predicted by the simplified plasma kinetic mechanism are consistent with the results of detailed mechanism, and the validation results are provided in Supplementary material in details. Meanwhile, the error divergence of energy transfer during mechanism simplification versus the number of reactions retained in the skeletal mechanism is display in Fig. 2. The results show that although large amount of species and reactions have been removed from detailed mechanism, the current compact skeletal mechanism has capability of reflecting the PAI process. Meanwhile, the modeling accuracy is further verified via the relative low errors (within 10%) in energy branches after simplification. In general, the compact and robust skeletal mechanism of PAI on methane is successfully built, and it is in good agreement of combustion characteristics with predictions by detailed mechanism.

3. Modeling of SDBD discharge by two-dimensional solver PASSKEy

As mentioned above, PASSKEy is a 2D plasma solver coupled with

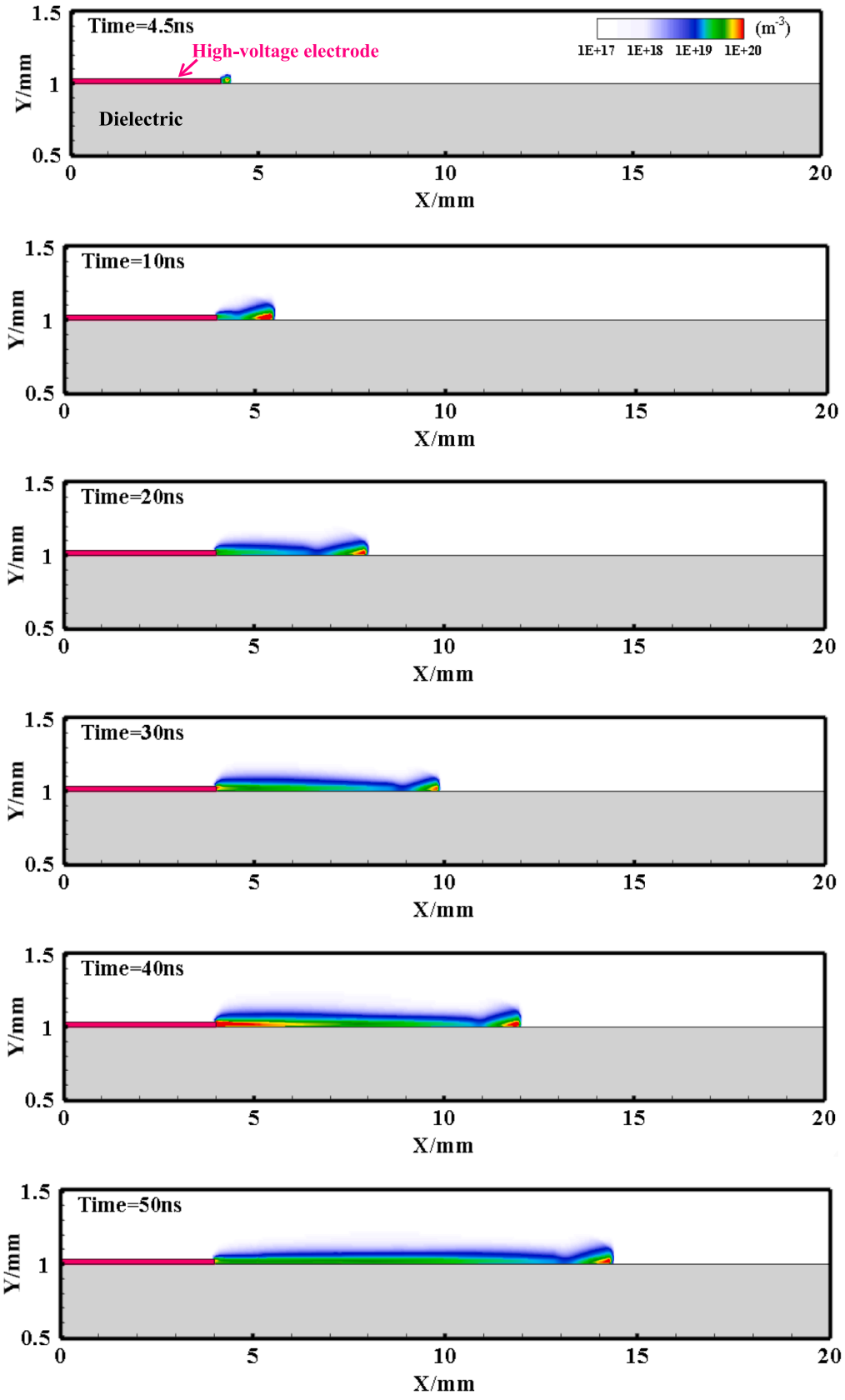

Fig. 5. The space–time evolution of the electron density (m^{-3}) for positive polarity streamers during CH_4/O_2/He SDBD discharge.

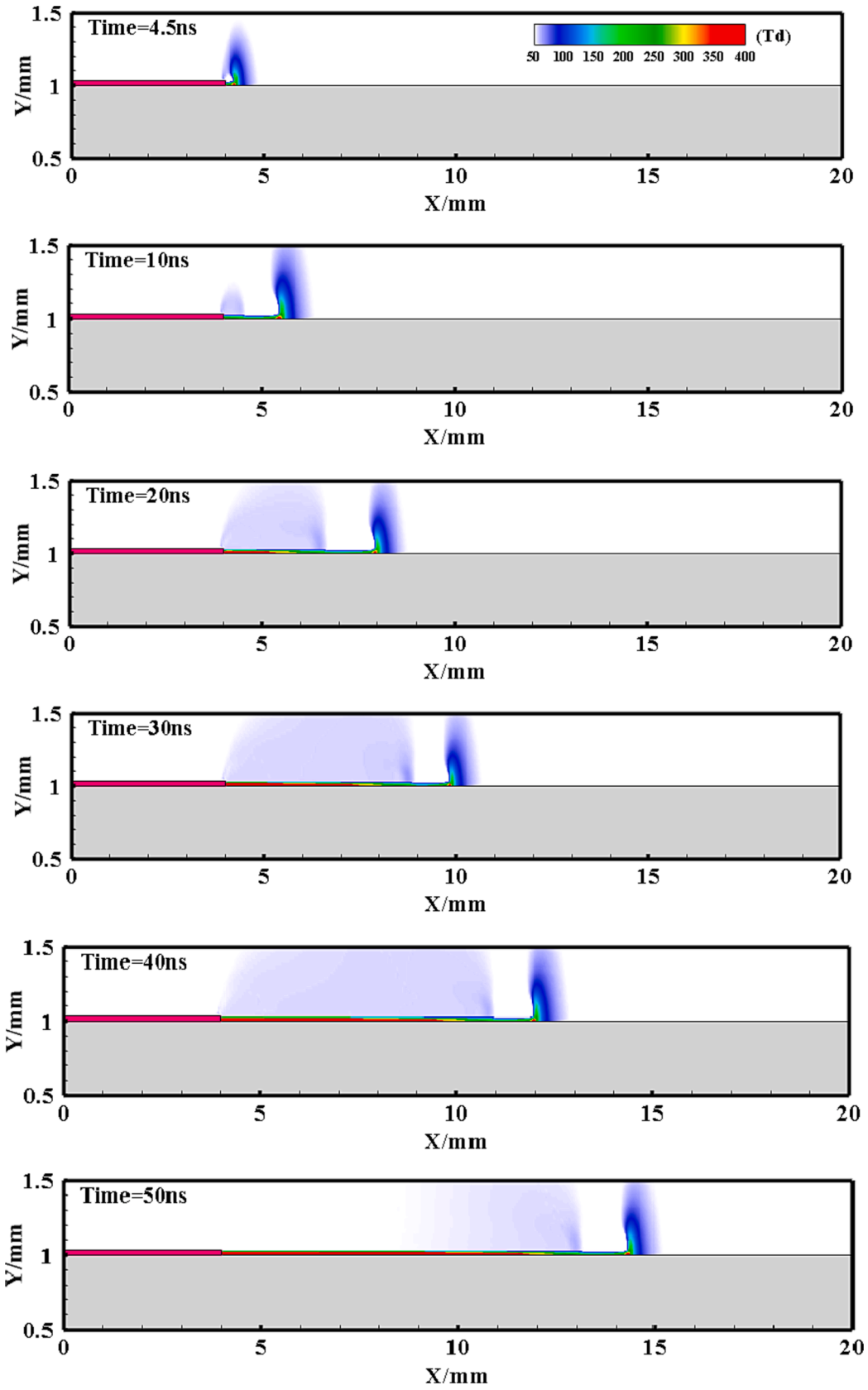

Fig. 6. The space–time evolution of the E/N (Td) for positive polarity streamers during CH_4/O_2/He SDBD discharge.

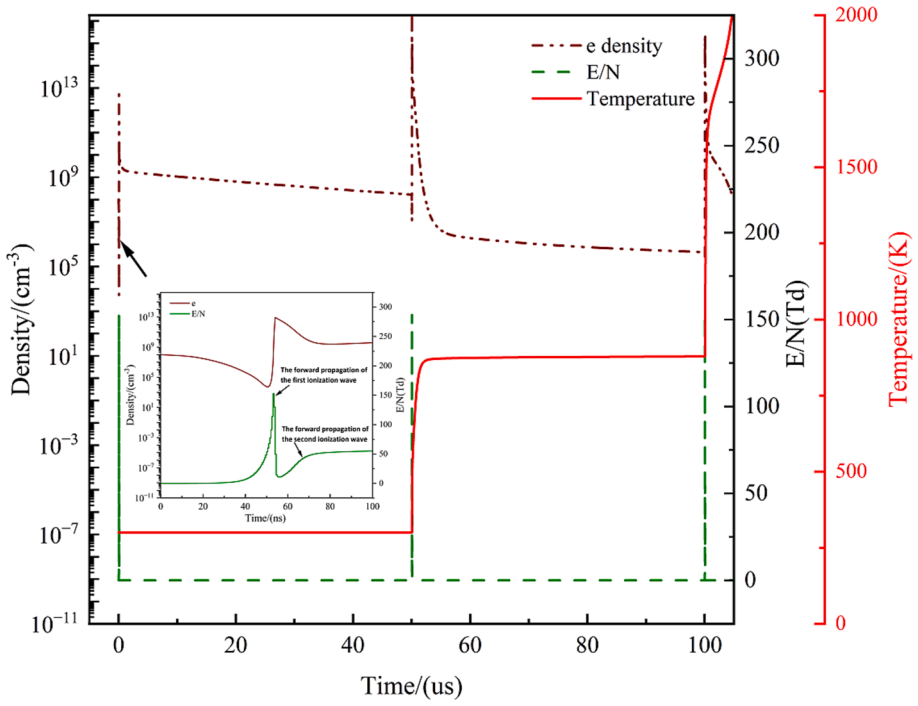

Fig. 7. Time evolution of electron density, E/N and gas temperature for PRF = 20 kHz and φ = 1(0.083CH_4/0.167O_2/0.75He).

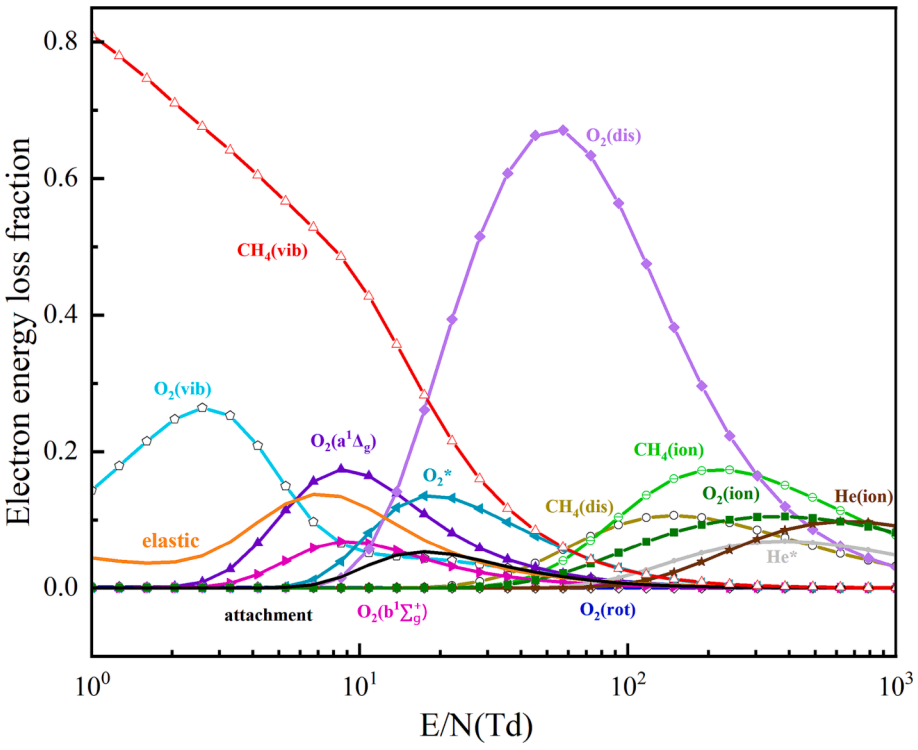

Fig. 8. The electron energy loss fraction as a function of E/N in a stoichiometric CH_4/O_2/He mixture(0.083CH_4/0.167O_2/0.75He).

flux equations, Poisson's equation and photoionization model. In this section, the simplified plasma mechanism proposed in the previous section is applied with PASSKEy code to simulate SDBD discharge characteristics. The numerical study is conducted in a stoichiometric CH_4/O_2/He (0.083CH_4/0.167O_2/0.75He) mixture at 300 K and atmospheric pressure. Helium is used as the dilution gas for improving the uniformity of the discharge. The voltage waveform and electrode shape are consistent with the experiment in our laboratory, in which nanosecond pulses are generated by parameterized pulsed power supply (HVP-20P, Xi'an Lingfengyuan Electronic Technology Co., Ltd.). The schematic diagram of electrode shape and computational domain with mesh layout is given in Fig. 3. The initial electron density is set to 10^8 cm^{-3} based on the given power density by formula (4), where P is power density of discharge space, e is elementary charge, n_e is the density of electrons, u_e is the mobility of electron and E is the strength of electric field. The same ion density is set due to quasi-neutrality of plasma.

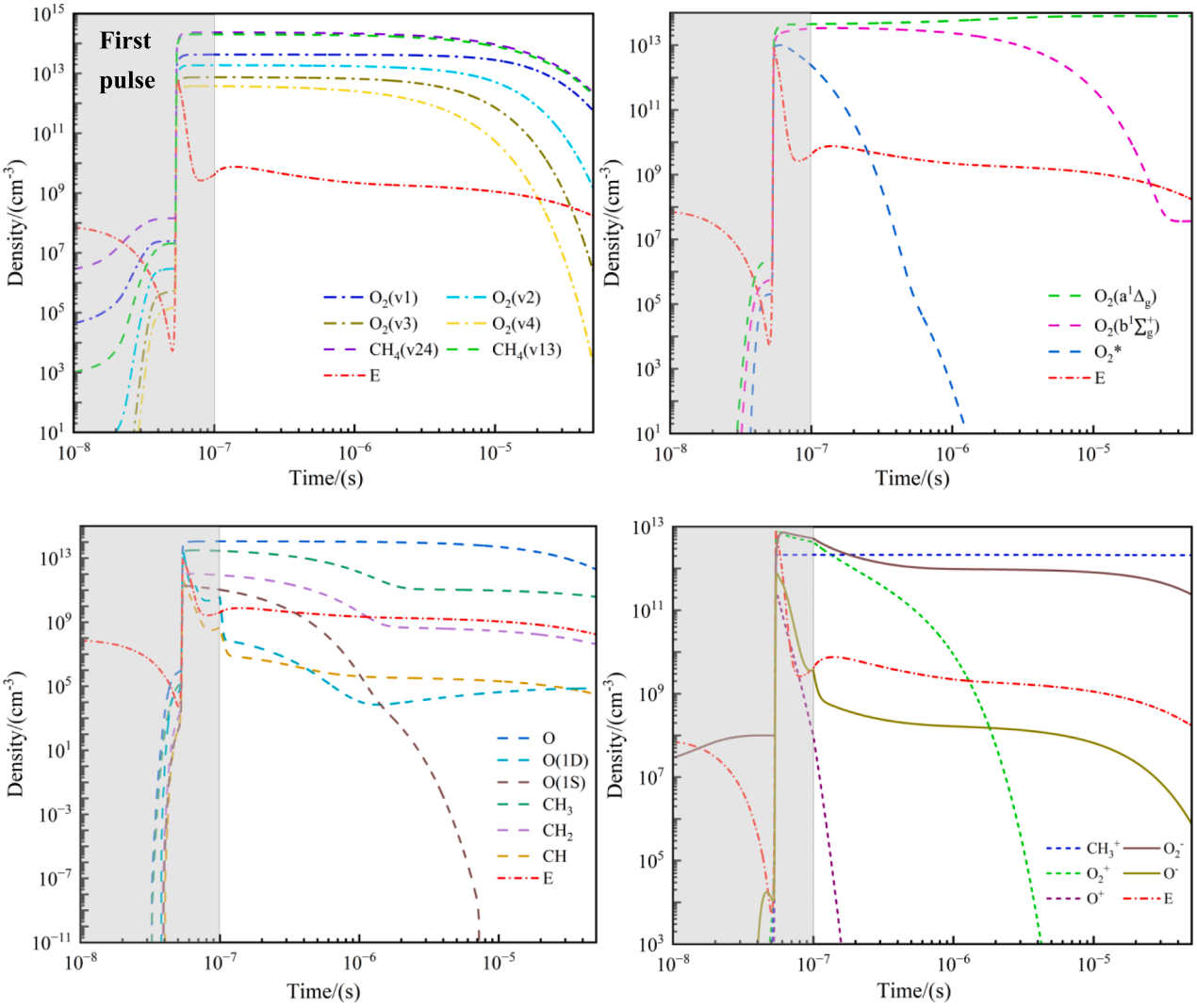

Fig. 9. Time evolution of excited species, radicals, ions and electrons density within the first pulse cycle for PRF = 20 kHz and φ = 1. The region in grey indicates discharge pulse stage.

$$P = e \times n_e \times u_e \times E^2 \quad (4)$$

The applied voltage along with measured and predicted current is given in Fig. 4. It is clear that the rising and falling edges each generate a discharge, the rising edge discharge is dominated by the driving voltage, while the falling edge discharge is caused by residual charges. A similar pattern of results was also observed in experimental study of Zhao Q [37]. The predicted current agrees well with the measurements in peak value and shapes, indicating good accuracy of the two-dimensional plasma discharge model.

For simplicity, in the subsequent calculations, the voltage is set to triangular waves of 15 kV in amplitude and 50 ns on the rising as well as falling edges as shown in Fig. 4. Fig. 5 and Fig. 6 demonstrate the space–time evolution of the electron density and E/N for positive streamers, respectively. The streamer approximately starts from intersection points of high-voltage electrode, dielectric and ambient gas due to "tip effect". A discharge channel with higher electron density is formed and it propagates along the dielectric surface after gas breakdown. The front edge of the discharge channel resembles a new electrode edge, which can maintain a high E/N and facilitate the outward growth of the discharge channel.

4. Simulation of ignition of CH_4/O_2/He mixture under the impact of NRP discharge

In this section, the effects of PRF on the ignition of CH_4/O_2/He mixture under varied equivalence ratios are simulated by ZDPlasKin-CHEMKIN model coupled with detailed mechanism. The numerical studies are conducted at 300 K and atmospheric pressure under constant volume adiabatic conditions. The electric field as an input continuous function for the zero-dimensional model, is called at dynamic time intervals. Duration nanosecond discharge, the electric field against time curve E(t) extracted at a probed point (x = 14.5, y = 1.1 mm) from discharge field by 2D PASSKEy model is interpolated. Moreover, E/N is set to zero at inter-pulse-intervals and plasma dynamics are ignored after ignition.

Fig. 7 shows the time evolution of electron density, E/N and gas temperature for PAI of stoichiometric CH_4/O_2 mixture with 75% helium dilution at PRF = 20 kHz. It can be observed that ignition occurs after three discharge pulses. The electron density shows a quasi-periodic change. The high temperature rise at the second pulse can be observed, mainly owing to dramatic increase in electron density leading to much greater deposited energy compared to the first pulse. The local magnification of Fig. 7 shows the time evolution of electron density and E/N during the first discharge pulse. The E/N at the probed point reaches two peaks within the discharge pulse, corresponding to the

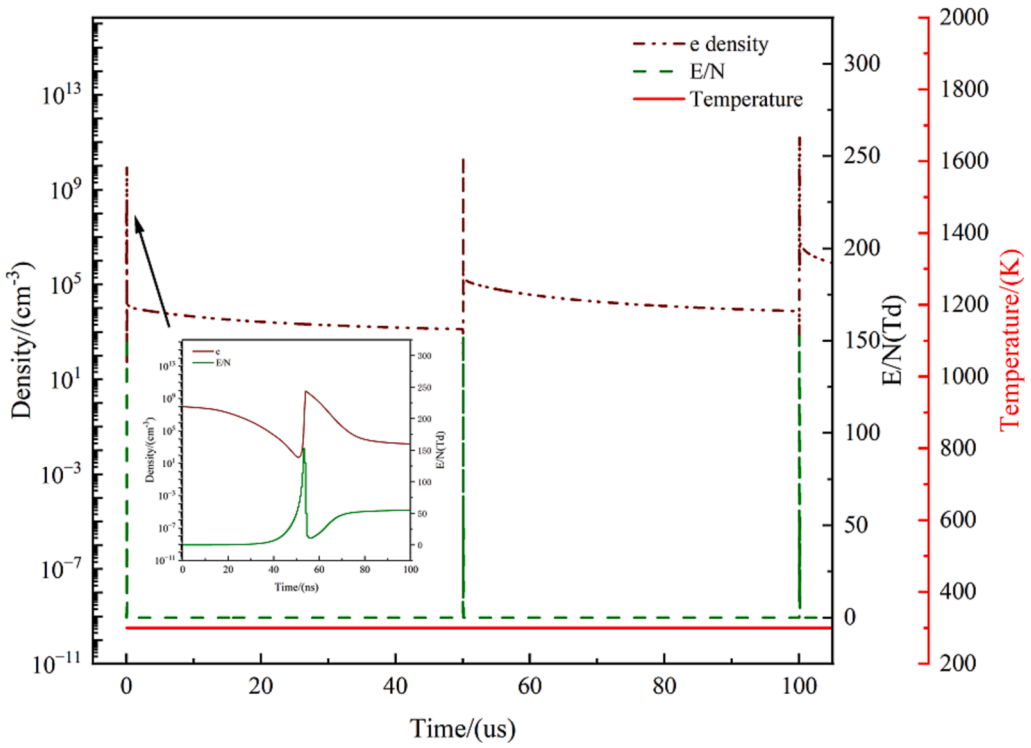

Fig.10. Time evolution of electron density, E/N and gas temperature for PRF = 20 kHz and φ = 0.5(0.05CH_4/0.20O_2/0.75He).

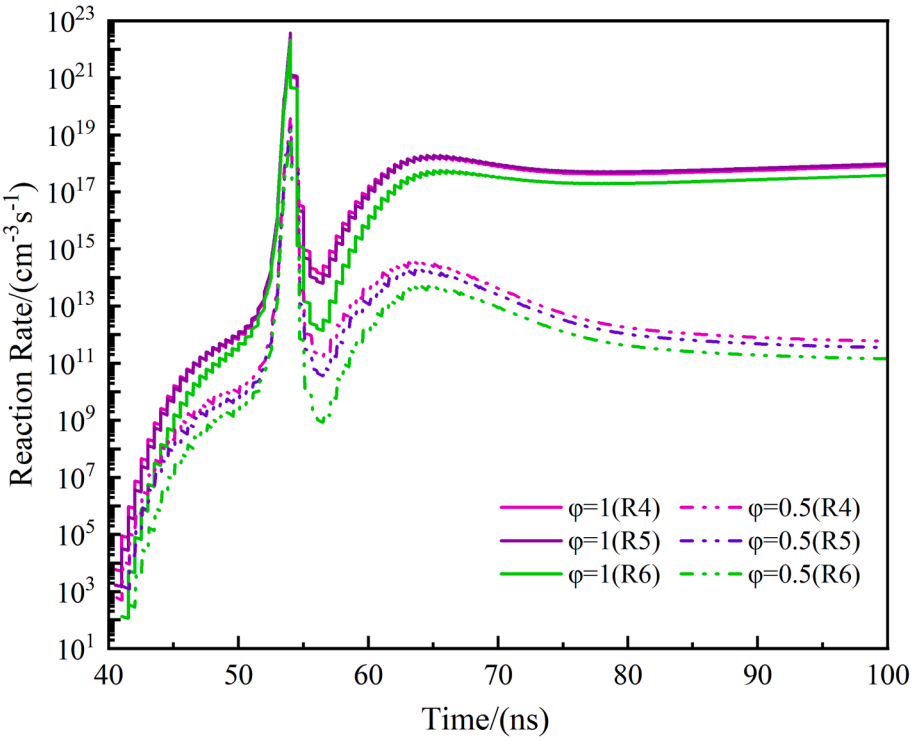

Fig. 11. The primary generation reaction rates of electrons under different equivalence ratios within the first discharge pulse.

propagation of the first and second ionization waves, respectively. The E/N is positively correlated with the average electron energy which is the dominant factor in controlling the type of electron collision reaction and the active species production. The trend of electron density variation can be explained by the electron energy loss fraction given in Fig. 8. The electron impact cross-sections are taken from LXCat online database, including datas for CH_4 [38], O_2 [39] and He [40]. The energy loss fractions are calculated by BOLSIG+ [41]. At the initial stage of discharge (0–50 ns), the electron attachment rate is greater than the ionization rate due to low E/N, resulting in the decrease of electron density. Due to the rapid increase in E/N caused by forward propagation of ionizing wave, the electron density quickly increases by eight orders

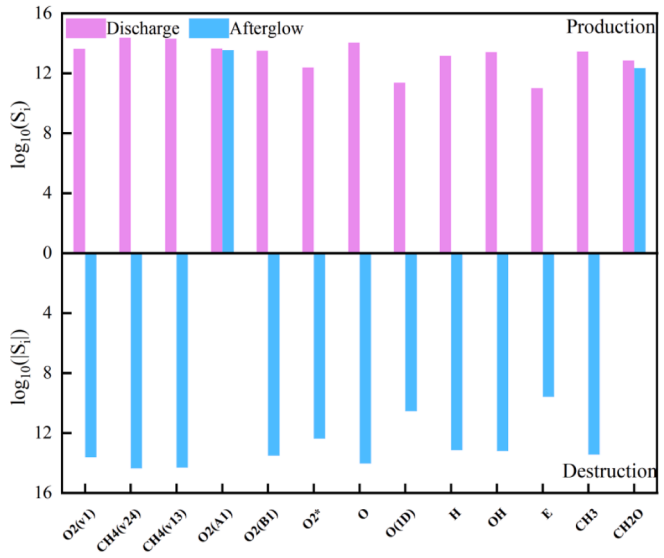

(a) φ=1,PRF=20kHz

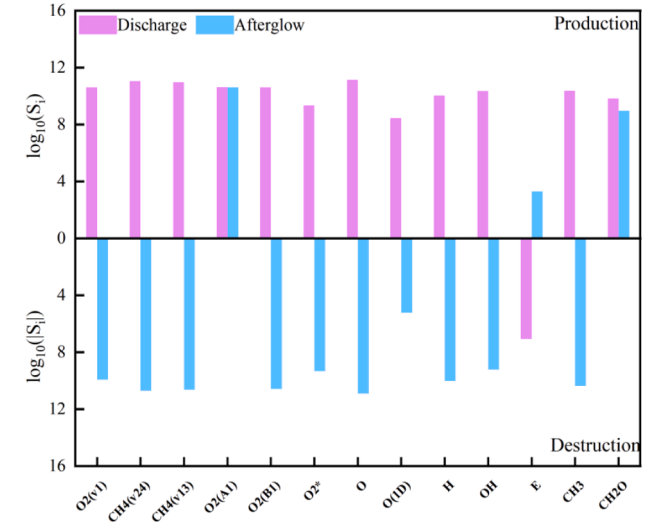

(b)φ=0.5,PRF=20kHz

Fig. 12. The species source terms in the first discharge pulse(pink bars) and its afterglow(blue bars) of excited species, active radicals and electrons for (a) φ = 1, PRF = 20 kHz and (b)φ = 0.5, PRF = 20 kHz. Top y-axis represents production and bottom y-axis represents destruction. Note:the units of source terms are in cm^{-3}, the logarithm of the (absolute) source terms is plotted.

of magnitude and reaches up to 10^{13} cm^{-3} after the ionization front, then decays immediately in the low reduced field below 50 Td.

The time evolution of excited species, radicals, ions and electrons density within the first pulse cycle is displayed in Fig. 9. The density of vibrationally excited species reaches to the peak during the pulse period and rapidly decreases after maintaining a stable cycle in the early afterglow stage. The density of species with lower vibrational levels such as O_2(v1) decreases slower, which is mainly maintained by the quenching reactions of vibrationally excited species with higher vibrational levels. $O_2(a^1\Delta_g)$ has a longer lifetime and higher density compared to $O_2\left(b^1\Sigma_g^+\right)$, which mainly comes from quenching of $O_2\left(b^1\Sigma_g^+\right)$ and electron impact excitation. The densities of O, O(1D), O(1S), CH_3, CH_2 and CH increase due to dissociation reactions under the influence of nanosecond pulses and then decrease in the subsequent afterglow stage. O atom has the highest peak density in excited species of oxygen atom and oxygen molecule. The density of electrons has a small increase in the early afterglow stage mainly owing to detachment reactions of negative ions through R1-R3 and shows exponential decay in the late afterglow. The positive ions O_2^+ and O^+ are rapidly quenched by electron–ion recombination reactions in the afterglow. The density of CH_3^+ has no significant changes after discharge which is maintained by quenching of excited states of He via $He^*+CH_4 \rightarrow He + CH_3^+ + H + e$. The densities of negative ions O_2^- and O^- rapidly decrease during the afterglow stage mainly due to ion-ion recombination reactions and collision reactions with neutral species such as reactions R1-R3.

$$R1: O_2^- + O => O_3 + E$$

$$R2: O_2^- + H => HO_2 + E$$

$$R3: O_2^- + O_2(b^1\Sigma_g^+) => O_2 + O_2 + E$$

Furthermore, the PAI characteristics on lean CH_4/O_2 mixture with 75% helium dilution at φ = 0.5 ($0.05CH_4/0.20O_2/0.75He$) is investigated. Considering the change of Electron Energy Distribution Function (EEDF) due to changed mixture compositions, the new space–time evolution of electric field from PASSKEy model is extracted at the point very close to original location. Fig. 10 shows the time evolution of electron density, E/N and gas temperature for PRF = 20 kHz and φ = 0.5. It is worthy to note that gas temperature has no significant change after three pulses. The electron density is three orders of magnitude lower than which conducted in a stoichiometric CH_4/O_2/He mixture. From the reaction pathway analysis, the electrons are generated mainly owing to ionization reactions R4-R6.

$$R4: E + O_2 \rightarrow E + E + {O_2}^+;$$

$$R5: E + CH_4 \rightarrow E + E + {CH_4}^+;$$

$$R6: E + CH_4 \rightarrow E + E + {CH_3}^+ + H;$$

The primary generation reaction rates of electrons in R4-R6 are plotted in Fig. 11 for the case of φ = 0.5 and φ = 1.0 at the same PRF within the first discharge pulse. It can be observed that the case for φ = 1 is more conducive to the occurrence of ionization reactions. The number of electrons has a direct impact on the production of active species under the same mean electron energy. In addition, the net production, net consumption of excited species, active radicals and electrons in the first discharge pulse and its afterglow (The time range from pulse-off to next pulse-on) under two equivalence ratios at PRF = 20 kHz are counted in Fig. 12. It can be observed that the decrease in the number of electrons directly affects the production of active particles during pulse discharge, therefore, the plasma kinetic effect has weakened to a great extent, which directly leads to the failure of ignition after three pulses when the equivalence ratio is decreased to 0.5.

To enhance the PAI effect on relative lean fuel mixture, a burst of repetitive pulses (PRF = 100 kHz) with more active species and radical pool accumulated via inter-pulse coupling is applied in this study. Fig. 13 plots the time evolution of electron density, E/N and gas temperature for CH_4/O_2/He mixture at PRF = 100 kHz and φ = 0.5. It was indicated that ignition occurs after five discharge pulses. The electron density increases due to the shortened pulse interval, which has a direct impact on the generation of active particles. From this standpoint, it is speculated that the density of “short lifetime” species which play a significant role in promoting the ignition process and accelerating the combustion chain reactions has enriched due to the intensive repetitive pulses.

To further investigate the major sources of key particles dominated in PAI of CH_4/O_2/He mixture, the reaction path diagrams are elaborately depicted based on contribution rate of each reaction to the

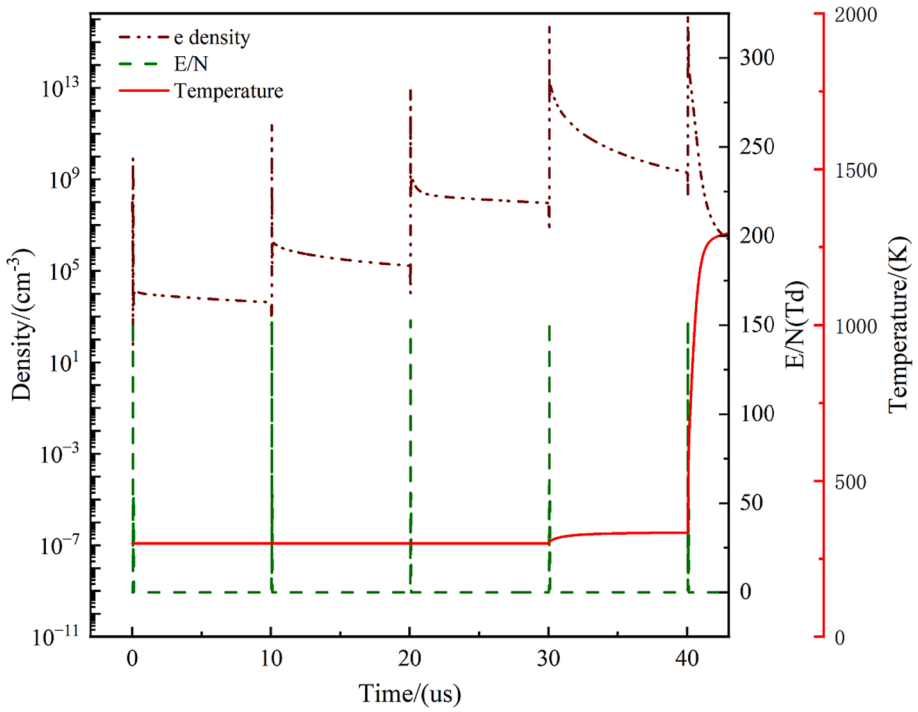

Fig. 13. Time evolution of electron density, E/N and gas temperature for PRF = 100 kHz and φ = 0.5 (0.05CH_4/0.20O_2/0.75He).

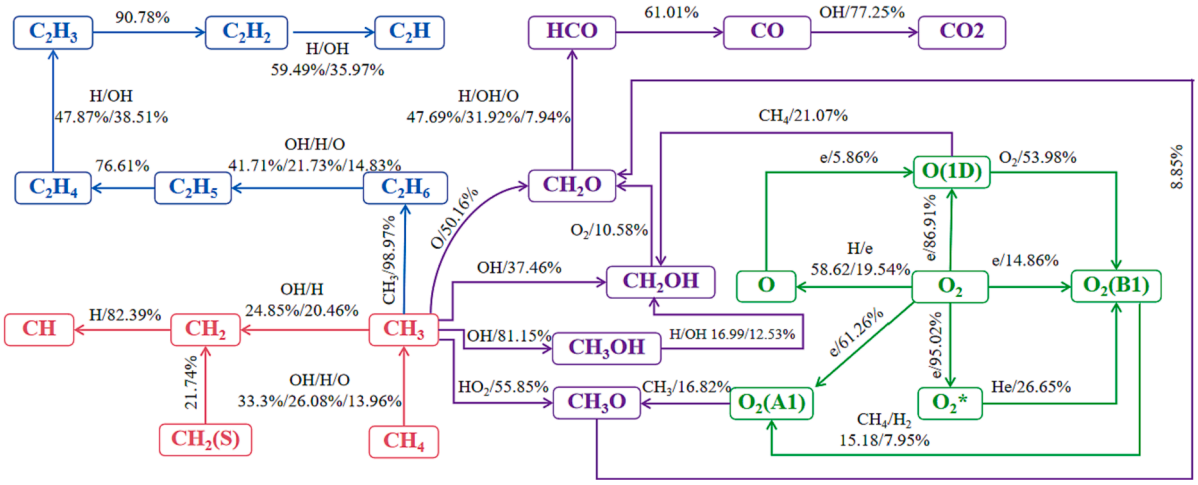

Fig. 14. The reaction path diagram for φ = 1 and PRF = 20 kHz (The number on the line represents the contribution rate of each reaction to generation of particle).

particles in Fig. 14 (φ = 1, PRF = 20 kHz) and Fig. 15 (φ = 0.5, PRF = 100 kHz). The time range from the start of the first discharge pulse to the ignition time is counted in the reaction paths analysis. Non-equilibrium plasma promotes the production of active species such as O atoms, singlet oxygen atoms O(1D) and singlet oxygen molecule $O_2(a^1\Delta_g)$, which accelerate the generation of ignition intermediates CH_2O and HCO. O(1D) mainly comes from electron impact dissociation reaction via $E + O_2 \rightarrow E + O + O(1D)$, while most of $O_2(a^1\Delta_g)$ and O_2* are produced from electronic excitation reactions via $E + O_2 \rightarrow E + O_2(a^1\Delta_g)$ and $E + O_2 \rightarrow E + O_2$*, respectively. $O_2\left(b^1\Sigma_g^+\right)$ is mainly originated from quenching of O(1D) via $O(1D) + O_2 \rightarrow O + O_2(b^1\Sigma_g^+)$. The most noteworthy feature of the path is that the source of O atoms is different for φ = 1, PRF = 20 kHz and φ = 0.5, PRF = 100 kHz. For φ = 1, PRF = 20 kHz, O atoms mainly comes from $H + O_2 \rightarrow O + OH$ via chemical effect. For φ = 0.5, PRF = 100 kHz, most of O atoms are derived from electron impact dissociation reactions $E + O_2 \rightarrow E + O + O/O(1D)$, quenching of $O_2\left(b^1\Sigma_g^+\right)$ via$O_2\left(b^1\Sigma_g^+\right) + H \rightarrow OH + O$, quenching of O(1D) via $O(1D) + O_2 \rightarrow O + O_2\left(b^1\Sigma_g^+\right)$. Moreover, CH_3 is outstanding towards the formation of C_2Hy and CH_2O. It is noteworthy that two additional active particles participant paths have been involved to the sources of CH_3 at φ = 0.5, PRF = 100 kHz, via $CH_4(v13) + O \rightarrow CH_3 + OH$ and $O(1D) + CH_4 \rightarrow CH_3 + OH$ respectively. As a consequence, it can be concluded that the shortened pulse interval period is a more promising way to enrich the concentration of active species that are rapidly quenched during the afterglow stage but have a promoting effect on ignition, thereby strengthening the plasma kinetic effect.

5. Conclusions

The effects of NRP-SDBD plasma on the stimulating ignition of varied CH_4/O_2/He mixtures are numerically studied. Main conclusions can be

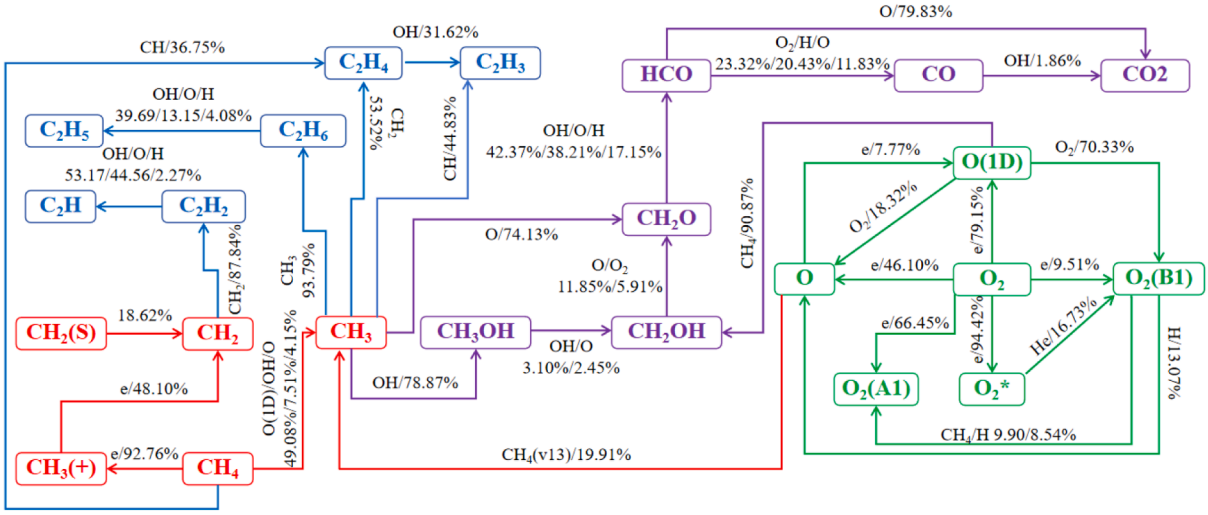

Fig. 15. The reaction path diagram for φ = 0.5 and PRF = 100 kHz (The number on the line represents the contribution rate of each reaction to generation of particle).

drawn from this work, as follows:

1. A skeletal plasma kinetic mechanism of CH_4/O_2/He with 91 reactions has been proposed based on P-DRGEP method and consumption path flux analysis. Energy branching are reproduced with less than 10% error, together with good agreement on predicted gas temperature. Overall, the physical properties of plasma discharge are well calibrated, providing fundamentals for the subsequent PAI numerical simulations.
2. Coupled with plasma kinetics and Poisson's equation, a two-dimensional simulation of plasma discharge process via PASSKEy is performed and verified through measured current. The sequential and spatial E/N depending on the propagation of streamers during nSDBD process is captured, and its evolution determines the production of active species for ignition enhancement.
3. A zero-dimensional ZDPlasKin-CHEMKIN model is used to study the effects of different PRF on the low temperature ignition of CH_4/O_2/He mixture under different equivalence ratios. It is suggested that the less electrons are generated in lean mixture thereby weakening the plasma kinetic effects. Intensive RPF facilitates the effects of interpulse coupling and therefore effectively promotes ignition.
4. Active species such as O, O(1D), $O_2(a^1\Delta_g)$ generated by non-equilibrium plasma accelerate the rates of chain reactions and the consequent production of ignition intermediates CH_2O and HCO. It is noteworthy that for the case of φ = 1 and PRF = 20 kHz, O atoms mainly comes from $H + O_2 \rightarrow O + OH$ via chemical effect, while for the case of φ = 0.5 and PRF = 100 kHz, most of O atoms are derived from electron impact dissociation and quenching reactions. Two additional plasma reactions have been involved to the main sources of CH_3 at φ = 0.5, PRF = 100 kHz, via $CH_4(v13) + O \rightarrow CH_3 + OH$ and $O(1D) + CH_4 \rightarrow CH_3 + OH$, respectively.

CRediT authorship contribution statement

Ziying Xin: Writing – review & editing, Visualization, Software, Investigation, Data curation. **Zhencao Zheng:** Investigation, Conceptualization. **Yong Hu:** Investigation, Conceptualization. **Ao Sun:** Investigation, Conceptualization. **Feiyang Zhao:** Writing – review & editing, Visualization, Supervision, Funding acquisition, Conceptualization. **Wenbin Yu:** Supervision, Funding acquisition, Conceptualization.

Declaration of Competing Interest

The authors declare that they have no known competing financial interests or personal relationships that could have appeared to influence the work reported in this paper.

Data availability

No data was used for the research described in the article.

Acknowledgement

The authors greatly acknowledge the support of Shandong Provincial Natural Science Foundation (No. ZR2022QE268 and No. 2022HWYQ-061) and Guangdong Basic and Applied Basic Research Foundation (No. 2022A1515110571).

Appendix A. Supplementary material

Supplementary data to this article can be found online at https://doi.org/10.1016/j.fuel.2023.129975.

References

[1] Park S, Lee M, Bae J, et al. Plasma-assisted non-oxidative conversion of methane over Mo/HZSM-5 catalyst in DBD reactor. Top Catal 2017;60:735–42.
[2] Ju Y, Sun W. Plasma assisted combustion: Dynamics and chemistry. Prog Energy Combust Sci 2015;48:21–83.
[3] Ju Y, Sun W. Plasma assisted combustion: Progress, challenges, and opportunities. Combust Flame 2015;162(3):529–32.
[4] Ju Y, Lefkowitz JK, Reuter CB, et al. Plasma assisted low temperature combustion. Plasma Chem Plasma Process 2016;36:85–105.
[5] Popov NA. Kinetics of plasma-assisted combustion: effect of non-equilibrium excitation on the ignition and oxidation of combustible mixtures. Plasma Sources Sci Technol 2016;25(4):043002.
[6] Starikovskiy A, Aleksandrov N, Rakitin A. Plasma-assisted ignition and deflagration-to-detonation transition. Philos Trans R Soc A Math Phys Eng Sci 1960;2012(370):740–73.
[7] Zhao H, Zhao N, Zhang T, et al. Studies of multi-channel spark ignition of lean n-pentane/air mixtures in a spherical chamber. Combust Flame 2020;212:337–44.
[8] Sun J, Tang Y, Li S. Plasma-assisted stabilization of premixed swirl flames by gliding arc discharges. Proc Combust Instit 2021; 38(4): 6733-6741.
[9] Zhang R, Liao H, Yang J, et al. Exploring chemical kinetics of plasma assisted oxidation of dimethyl ether (DME). Combust Flame 2021;225:388–94.
[10] Sun J, Chen Q, Guo Y, et al. Quantitative behavior of vibrational excitation in AC plasma assisted dry reforming of methane. J Energy Chem 2020;46:133–43.
[11] Mao X, Chen Q, Guo C. Methane pyrolysis with N2/Ar/He diluents in a repetitively-pulsed nanosecond discharge: Kinetics development for plasma assisted combustion and fuel reforming. Energ Conver Manage 2019;200:112018.

[12] Suess M, Guenthner M, Schenk M, et al. Investigation of the potential of corona ignition to control gasoline homogeneous charge compression ignition combustion. Proc Instit Mech Eng, Part D: J Automobile Eng 2012;226(2):275–86.
[13] Cruccolini V, Discepoli G, Cimarello A, et al. Lean combustion analysis using a corona discharge igniter in an optical engine fueled with methane and a hydrogen-methane blend. Fuel 2020;259:116290.
[14] Wang Z, Huang J, Wang Q, et al. Experimental study of microwave resonance plasma ignition of methane–air mixture in a constant volume cylinder. Combust Flame 2015;162(6):2561–8.
[15] Ono R, Ogura K, Mogi T. Stabilization of premixed lean methane-air combustion using dielectric barrier discharge with low pollutant emissions. J Phys D Appl Phys 2017;50(36):365201.
[16] Cruccolini V, Discepoli G, Ricci F, et al. Comparative analysis between a barrier discharge igniter and a streamer-type radio-frequency corona igniter in an optically accessible engine in lean operating conditions[R]. SAE Technical Paper, 2020.
[17] Yu J, He L, Ding W, et al. Research on the impacts of air temperature on the evolution of nanosecond pulse discharge products. Appl Therm Eng 2016;98:265–70.
[18] Soloviev VR, Krivtsov VM, Shcherbanev SA, et al. Evolution of nanosecond surface dielectric barrier discharge for negative polarity of a voltage pulse. Plasma Sources Sci Technol 2016;26(1):014001.
[19] Starikovskii AY, Nikipelov AA, Nudnova MM, et al. SDBD plasma actuator with nanosecond pulse-periodic discharge. Plasma Sources Sci Technol 2009;18(3):034015.
[20] Ding C, Jean A, Popov NA, et al. Fine structure of streamer-to-filament transition in high-pressure nanosecond surface dielectric barrier discharge. Plasma Sources Sci Technol 2022;31(4):045013.
[21] Bayoda KD, Benard N, Moreau E. Nanosecond pulsed sliding dielectric barrier discharge plasma actuator for airflow control: Electrical, optical, and mechanical characteristics. J Appl Phys 2015;118(6):063301.
[22] Abdelaziz AA, Ishijima T, Seto T, et al. Characterization of surface dielectric barrier discharge influenced by intermediate frequency for ozone production. Plasma Sources Sci Technol 2016;25(3):035012.
[23] Zembi J, Cruccolini V, Mariani F, et al. Modeling of thermal and kinetic processes in non-equilibrium plasma ignition applied to a lean combustion engine. Appl Therm Eng 2021;197:117377.
[24] Mao X, Chen Q, Rousso AC, et al. Effects of controlled non-equilibrium excitation on H2/O2/He ignition using a hybrid repetitive nanosecond and DC discharge. Combust Flame 2019;206:522–35.
[25] Mao X, Rousso A, Chen Q, et al. Numerical modeling of ignition enhancement of CH4/O2/He mixtures using a hybrid repetitive nanosecond and DC discharge. Proc Combust Inst 2019;37(4):5545–52.
[26] Faingold G, Lefkowitz JK. A numerical investigation of NH3/O2/He ignition limits in a non-thermal plasma. Proc Combust Instit 2021; 38(4): 6661-6669.
[27] Zhong H, Shneider MN, Mokrov MS, et al. Thermal-chemical instability of weakly ionized plasma in a reactive flow. J Phys D Appl Phys 2019;52(48):484001.
[28] Kulikovsky AA. Positive streamer in a weak field in air: A moving avalanche-to-streamer transition. Phys Rev E 1998;57(6):7066.
[29] Stepanyan SA, Soloviev VR, Starikovskaia SM. An electric field in nanosecond surface dielectric barrier discharge at different polarities of the high voltage pulse: spectroscopy measurements and numerical modeling. J Phys D Appl Phys 2014;47(48):485201.
[30] Soloviev VR, Krivtsov VM. Surface barrier discharge modelling for aerodynamic applications. J Phys D Appl Phys 2009;42(12):125208.
[31] Zhu Y, Shcherbanev S, Baron B, et al. Nanosecond surface dielectric barrier discharge in atmospheric pressure air: I. measurements and 2D modeling of morphology, propagation and hydrodynamic perturbations. Plasma Sources Sci Technol 2017;26(12):125004.
[32] Chen X, Zhu Y, Wu Y. Modeling of streamer-to-spark transitions in the first pulse and the post discharge stage. Plasma Sources Sci Technol 2020;29(9):095006.
[33] Mao X, Zhong H, Zhang T, et al. Modeling of the effects of non-equilibrium excitation and electrode geometry on H2/air ignition in a nanosecond plasma discharge. Combust Flame 2022;240:112046.
[34] Mao X, Zhong H, Wang Z, et al. Effects of inter-pulse coupling on nanosecond pulsed high frequency discharge ignition in a flowing mixture. Proc Combust Inst 2023;39(4):5457–64.
[35] Lefkowitz JK, Guo P, Rousso A, et al. Species and temperature measurements of methane oxidation in a nanosecond repetitively pulsed discharge. Philos Trans R Soc A Math Phys Eng Sci 2015;373(2048):20140333.
[36] Bellemans A, Kincaid N, Deak N, et al. P-DRGEP: a novel methodology for the reduction of kinetics mechanisms for plasma-assisted combustion applications. Proc Combust Inst 2021;38(4):6631–9.
[37] Zhao Q, Xiong Y, Yang X, et al. Experimental study on multi-channel ignition of propane-air by transient repetitive nanosecond surface dielectric barrier discharge. Fuel 2022;324:124723.
[38] IST-Lisbon database, www.lxcat.net, retrieved on April 28, 2023.
[39] Phelps database, www.lxcat.net, retrieved on April 28, 2023.
[40] Biagi-v7.1 database, www.lxcat.net, retrieved on April 28, 2023.
[41] Hagelaar GJM, Pitchford LC. Solving the Boltzmann equation to obtain electron transport coefficients and rate coefficients for fluid models. Plasma Sources Sci Technol 2005;14(4):722–33.